Wind and Structures, Vol. 5, No. 5 (2002) 393-406
DOI: http://dx.doi.org/10.12989/was.2002.5.5.393

Wind loads on a solar array

G. A. Kopp† and D. Surry‡

Boundary Layer Wind Tunnel Laboratory, Faculty of Engineering Science, University of Western Ontario, London, ON, N6A 5B9, Canada

K. Chen‡†

Photovoltaics International LLC, Sunnyvale, CA, 94086, USA

Abstract. Aerodynamic pressures and forces were measured on a model of a solar panel containing six slender, parallel modules. Of particular importance to system design is the aerodynamically induced torque. The peak system torque was generally observed to occur at approach wind angles near the diagonals of the panel (45°, 135°, 225° and 315°) although large loads also occurred at 270°, where wind is in the plane of the panel, perpendicular to the individual modules. In this case, there was strong vortex shedding from the in-line modules, due to the observation that the module spacing was near the critical value for wake buffeting. The largest loads, however, occurred at a wind angle where there was limited vortex shedding (330°). In this case, the bulk of the fluctuating torque came from turbulent velocity fluctuations, which acted in a quasi-steady sense, in the oncoming flow. A simple, quasi-steady, model for determining the peak system torque coefficient was developed.

Key words: wind loads; solar array; vortex shedding; wake buffeting.

1. Introduction

Solar arrays are becoming more common both in terms of electrical power generation for sale by commercial power retailers and for local consumption in offices and factories to offset power costs during peak periods. This paper considers a design for the latter usage, based on panels of slender, parallel modules which track the sun allowing for optimum power generation over longer periods. They are appearing in many new building developments where they are often mounted on roofs.

The solar arrays under consideration here are usually made up of one or more panels, each panel consisting of several modules that are driven by a single motor and gearing system. The motor and gearing system used in tracking the sun drive all of the panels modules in a single system. Thus, any torque that is simultaneously applied to all modules could cause serious mechanical problems to the drive system. Since the modules are typically asymmetric in shape, the tracking system could be susceptible to large wind-induced torques from the groups of modules in the panel if the response of the individual modules is highly correlated in the wind. This has lead to failures of the gearing in the drive system. Compounding the problem is that the centre of rotation for the individual modules is often chosen

† Associate Professor and Associate Research Director
‡ Professor and Research Director
‡† Associate Engineer

based on factors other than the minimization of the wind-induced torque. Currently, there are no wind load provisions for precisely this type of structure, so the present work is concerned with defining basic wind loads.

Flow around arrays and the individual modules is quite complicated for several reasons. First, the arrays are often mounted on roofs so the wind loading will depend on building geometry and location as well as the precise location of the array on the roof. Second, the modules in typical arrays are spaced closely together with gaps being typically about two module diameters. This spacing is conducive to lock-in of the vortex shedding between modules which could lead to wake buffeting problems (e.g., Vickery 1981, Hangan and Vickery 1999). However, since the wind can come from any direction, wake buffeting may not be the major cause of high system loads. In addition, since the module angle changes as it tracks the sun, the intensity of the wind loads could also depend on the time of day that a wind occurs (although there likely would be a cloud cover during a design wind).

There have been few previous aerodynamic studies of solar arrays, the work of Cochran (1986) and Peterka and Derickson (1992) being notable exceptions. Cochran's work focused primarily on the frame loads for large arrays placed in turbulent boundary layers and, in particular, how porosity (i.e., openings between modules) might be used to reduce design loads. Peterka and Derickson focused on solid collectors, the loads on single isolated collectors, and fields of collectors used for large-scale (i.e., non-local) power generation. In contrast, the present work is focused on the total system torque found at the main drive gearbox for a particular porous solar array and its modules developed by PhotoVoltaics International (PVI). This type of array is generally designed for roof-top use on industrial buildings. Typical module lengths are 4 to 5 m. In contrast, the large ground-mounted arrays of Cochran (1986) and Peterka and Derickson (1992) are about three to five times as large and are typically placed in a field with multiple rows of panels[1]. A simple design model for the PVI system peak torque is presented based on the present experiments in uniform flow. No work has been done to estimate the effects of the location of the array on the roof, nor of the effects of the building geometry upon which the panels are usually located.

2. Experimental setup

A model of a photovoltaic concentrator panel that incorporates parallel slender modules was tested in a wind tunnel in order to determine the aerodynamic loads. The model, consisting of six modules and a frame, was constructed of acrylic at 1:6 scale. The modules were separated by 2.25 D where $D = 76$ mm and the length of the module, $L = 750$ mm. The model had moveable parts so that declination angle (γ), module angle (θ) and wind angle (β) could be easily changed. Fig. 1 shows the definition of these angles as well as the coordinate system used for each module (with the z-axis parallel to the module axis, in the direction towards the "bottom"). Fig. 2 shows a photograph of the model in the wind tunnel, as viewed from $\beta \sim 140^{\circ}$.

A total of 504 pressure taps were used on the six modules. These were distributed in 18 "rings", each ring with 28 taps. Fig. 3 shows the distribution of the taps around each ring. Note that the cooling fins near the bottom edges, modeled with styrene, did not have pressure taps placed on them. The tributary area of these fins was included in the analysis with the pressures assumed to be the same as the nearest adjacent tap. Three of the modules had five rings while the remaining three had one ring each, as shown

[1]Note that the panels may be mounted above ground, and that there may be fences around and within the field they are mounted in.

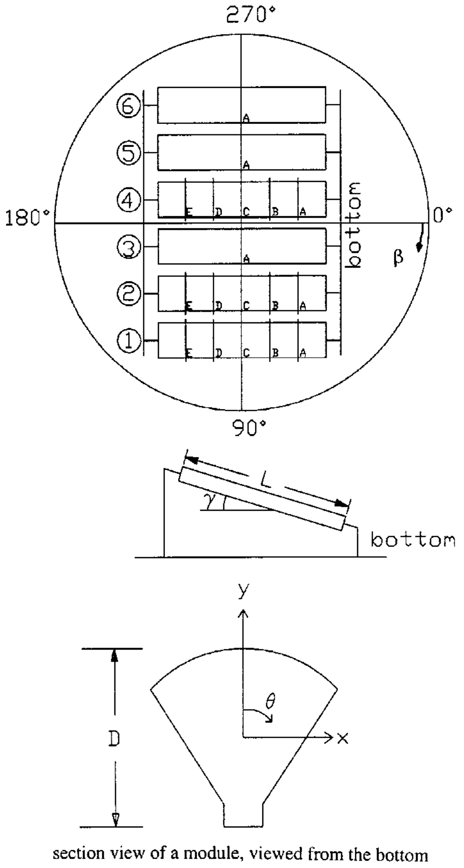

Fig. 1 A schematic sketch of the solar panel and the definition of wind angle, declination angle (γ), module angle (θ), and the length (L) and "diameter" (D) of the individual modules. Typical prototype sizes are $L \sim 4\text{-}5$ m and $D \sim 0.5$ m. Modules are labeled with number (shown to the left of each module), the rings of taps are labeled with letters. The z-axis is defined by the right-hand rule.

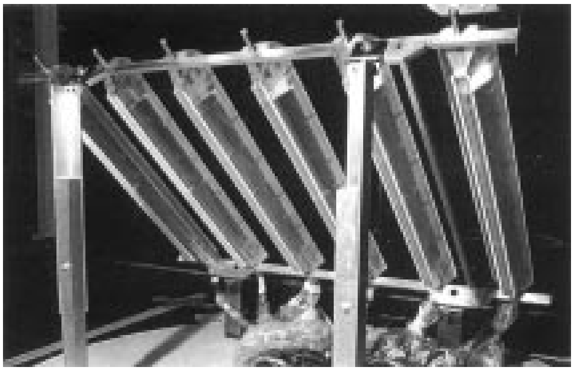

Fig. 2 A photograph of the model solar panel in the wind tunnel. The view is from a wind angle of about 140°

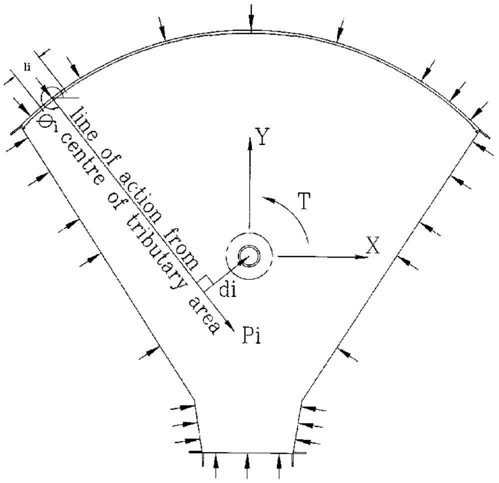

Fig. 3 A scaled drawing of the 28 pressure tap locations around a typical ring as viewed from the bottom of the panel. Also shown are a typical tributary area for one tap, and how the "torque arm" is computed from it

in the top of Fig. 1 and in Fig. 3. The rings are labeled such that module 1 - ring C is called ring 1C.

The model was mounted near the upstream end of the test section of the Boundary Layer Wind Tunnel II at the University of Western Ontario. A turbulence generating grid could be placed just upstream allowing both smooth and turbulent flow conditions to be examined. In smooth flow conditions, the streamwise turbulence intensity, $I\,(=u'/U$, where u' is the streamwise rms. velocity), is less than 1% at the model location while, with the upstream grid in place, the streamwise turbulence intensity is $I = 9\%$. The wind tunnel speed, U, was 15 m/s. The longitudinal length scale of the turbulence is of the order of the module spacing, and hence is too small by at least an order of magnitude in representing atmospheric turbulence, although real building-generated turbulence would also be of smaller scale. The intent of the experiments was to determine loads that could be

Table 1 Summary of the geometry and flow condition for the seven pressure tests

Test	Flow Type	γ	θ
A	smooth	45°	0°
B	smooth	45°	75°
C	smooth	45°	45°
D	smooth	30°	45°
E	smooth	30°	75°
F	smooth	10°	75°
G	turbulent	45°	75°

used with full-scale mean speeds, assuming a quasi-steady behaviour. Turbulence was introduced to determine the effects of fine-scale turbulence on the mean and vortex-induced loads.

The pressure signals were low pass filtered at 100 Hz and then sampled at 200 samples/sec per channel. In one model configuration (test A), the data was sampled for 160 sec in order to obtain autospectra. For the remaining tests the sampling time was 60 sec. Note that the tubing system had a frequency response which was flat to about 100 Hz.

For the present experiments, the Reynolds number was 7.6×10^4, where $U = 15$ m/s, $D = 76$ mm (D is defined in Fig. 1). This value is deemed adequate when compared to the possible range of full-scale Reynolds number. For example, for a full-scale wind speed of 50 mph, the Reynolds number is 6.6×10^5. Thus, the difference is about one order of magnitude, which should not be significant given the relatively sharp edges of the cross sectional shape, as can be seen in Figs. 2 and 3. The one place where there could be a Reynolds number problem would be on the curved surface of the modules. Considering the circular cylinder, for example, the Reynolds number effects on the aerodynamic forces, once Re is greater than about 10^3, are primarily on the location of separation points. However, the sharp edges at every corner will control the separation so that the differences between full-scale and model-scale results are expected to be minimal.

Seven separate sets of tests were performed to determine the effects of module angle (θ), declination angle (γ), wind angle (β) and turbulence level, as listed in Table 1. Six of the tests were performed in smooth flow conditions in order to separate the effects due to declination angle, module angle and wind angle from those due to turbulence. The configuration with $\gamma = 45^o$ and $\theta = 75^o$ degrees is chosen for detailed analysis in the present work, since this configuration tended to yield the worst loads (Kopp and Surry 1998). This configuration was used in two tests, namely, B and G for smooth and turbulent flow conditions, respectively. We will examine three wind angles in particular, 225°, 270° and 330°, because they exhibit a range of interesting phenomena. As will be seen, at a wind angle of 270° locked-in vortex shedding on all six modules leads to a large fluctuating system torque while at a wind angle of 330° this does not occur. In this case, the large observed system torque is due to a peak upstream turbulent velocity, which acts in a quasi-steady sense.

3. Pressure distribution

Figs. 4~5 depict the maximum ($\hat{C}_p$) minimum ($\check{C}_p$) and mean ($\overline{C}_p$) pressure coefficients from ring 1C in test G (turbulent flow, $\theta = 75^o$, and $\gamma = 45^o$) where the pressure coefficient, C_p, is

$$C_p = \frac{p - p_o}{q} \tag{1}$$

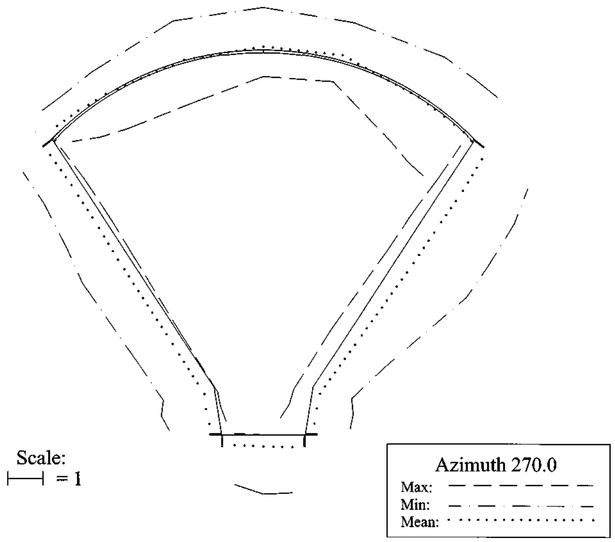

Fig. 4 Peak and mean pressure distributions for ring 1C in flow case G and a wind angle of 270°

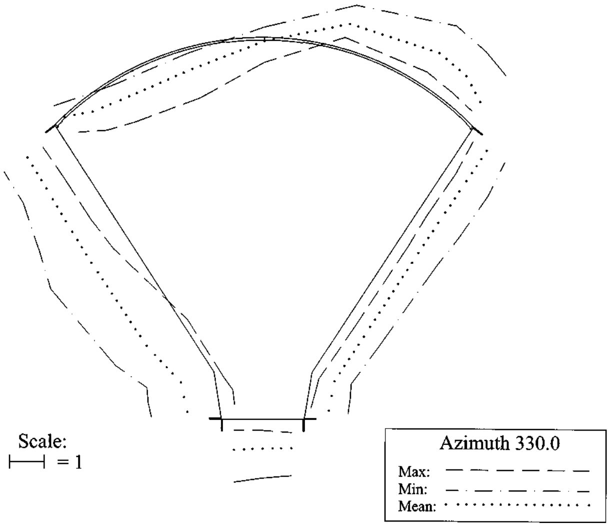

Fig. 5 Peak and mean pressure distributions for ring 1C in flow case G and a wind angle of 330°

p is the pressure measured at the tap, p_o is the static pressure and $q = (1/2)\rho U^2$, and ρ is the fluid density. Fig. 4 corresponds to a wind angle of 270°, Fig. 5 corresponds to 330°. Note that module 1 is at the trailing edge of the array for these angles. It does not "see" any undisturbed flow for $\beta = 270°$, although it does see some undisturbed oncoming flow for $\beta = 330°$.

For $\beta = 270°$, the mean pressure distribution is nearly symmetric and the magnitudes small because of the upstream blockage, as can be seen in Fig. 4. Thus, the mean torque about the centre of rotation (cf. Fig. 3) must be small. The maximum and minimum pressure coefficients are significantly larger, but are for the most part symmetric. It will be shown in subsequent sections that the fluctuating pressures are due to vortex shedding with corresponding instantaneous asymmetries in the pressure field yielding large system torque coefficients. In contrast, for $\beta = 330°$, shown in

Fig. 5, the mean pressure is not uniform, particularly on the curved surface, which contributes a net positive torque. The mean pressures on the other surfaces nearly cancel out. The stagnation point (where $\overline{C}_p = 1$) is observed to be on the left side of the upper curved surface, due to the module angle $\theta = 75^o$ and the declination angle $\gamma = 45^o$. The envelope of peak pressures show similar asymmetry and indicate that the peak values of torque are likely due to a similar pressure distribution as that causing the mean torque.

4. Wind-induced torque coefficients

4.1. Definition of torque coefficient

Unsteady aerodynamic loads were obtained by integrating the simultaneously sampled surface pressures. These integrations yield time histories of the coefficients for lift, drag and torque. In the present work, the focus is only on torque.

The torque is calculated as

$$T = C_T \, q \, L \, D^2 \tag{2}$$

where C_T is the torque coefficient,

$$C_T = \sum_{i=1}^{n} C_{pi} \frac{l_i d_i L_i}{D^2 L} sign_i \tag{3}$$

l_i is the tributary length around the module, L_i is the tributary length along the module, d_i is the perpendicular from the line of action of the pressure force through the centre of rotation, D is a normalizing length, L is the overall length of the module, and $sign_i$ is the sign of the torque caused by the pressure at tap i. These parameters are shown in Figs. 1 and 3.

4.2. Mean and RMS. torque coefficients on individual modules

Fig. 6 shows the values obtained for the mean torque coefficient, $\overline{C}_{T,i}$, and the rms. torque coefficient, $C'_{T,i}$, for the 6 midplane rings ($i = 1$-6) and the three modules with five rings ($i =$ "mod"). Two observations can be made regarding the mean coefficients. First, there is generally good agreement between the smooth flow and turbulent flow cases, although this is less so for the wind angle of 330^o than for 225^o and 270^o. Second, the coefficients are larger for the diagonal wind directions (225^o and 330^o) than for the perpendicular wind direction (270^o). This makes sense because for the diagonal wind directions, each module sees, to some extent, an undisturbed oncoming cross wind, whereas for the perpendicular case only the first module sees an undisturbed cross wind. This explains the relatively large coefficient observed for ring 6A for wind from 270^o. On the whole, the largest mean coefficients are observed for a wind angle of 330^o. In contrast, the perpendicular wind direction leads to the largest rms. coefficients, where Fig. 6 clearly shows that the largest values occur at a wind angle of 270^o. This is due to the strong wake buffeting from the locked-in vortex shedding for this particular wind direction, as shown in the next section.

4.3. Spectra and correlations

Figs. 7~9 depict autospectra of $C_{T,i}$ from the midplane rings of modules 1 and 6 for wind angles

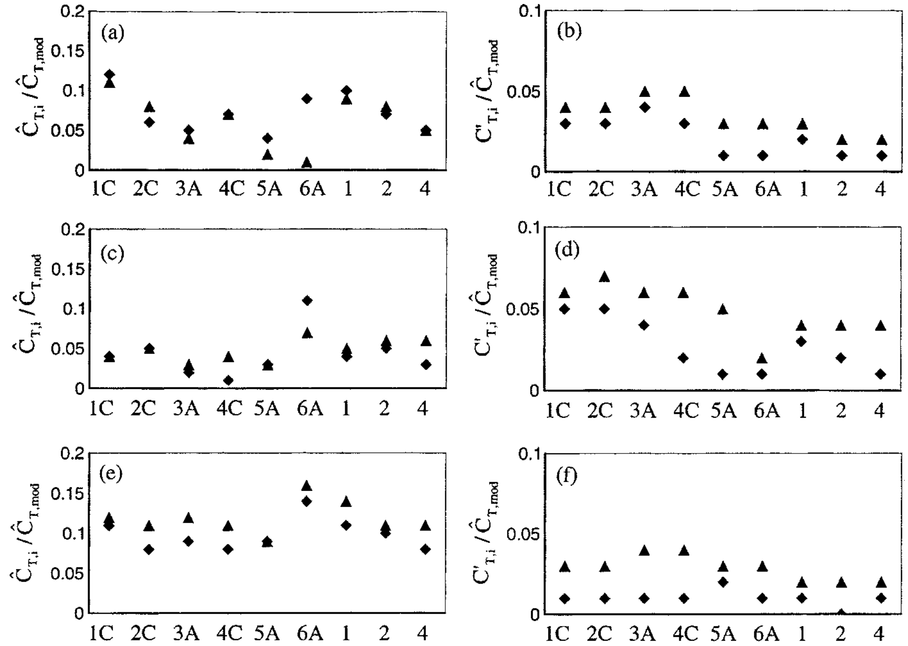

Fig. 6 Mean and rms. torque coefficients for the midplane rings and complete modules for wind angles of (a) 225°, (b) 225°, (c) 270°, (d) 270°, (e) 330° and (f) 330° in smooth (◆) and turbulent (▲) flow

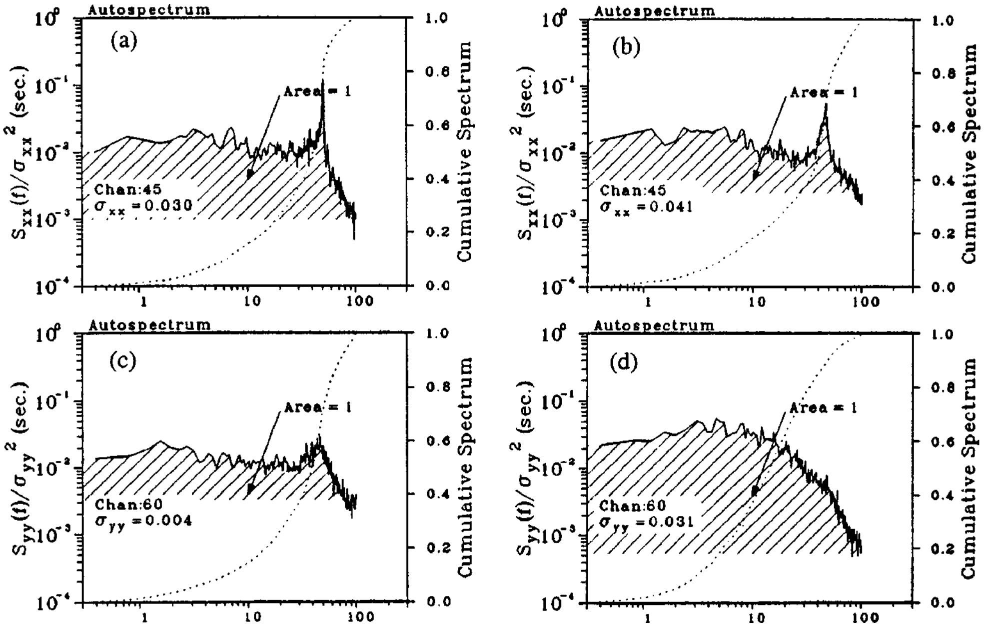

Fig. 7 Auto-spectra at a wind angle of 225° for (a) ring 1C in smooth flow (test B), (b) ring 1C in turbulent flow (test G), (c) ring 6A in smooth flow (test B) and (d) ring 6A in turbulent flow (test G)

of 225°, 270°, and 330°, respectively, in configurations B (smooth flow) and G (turbulent flow). For a wind angle of 225°, shown in Fig. 7, vortex shedding is observed at a frequency of 50 Hz. This

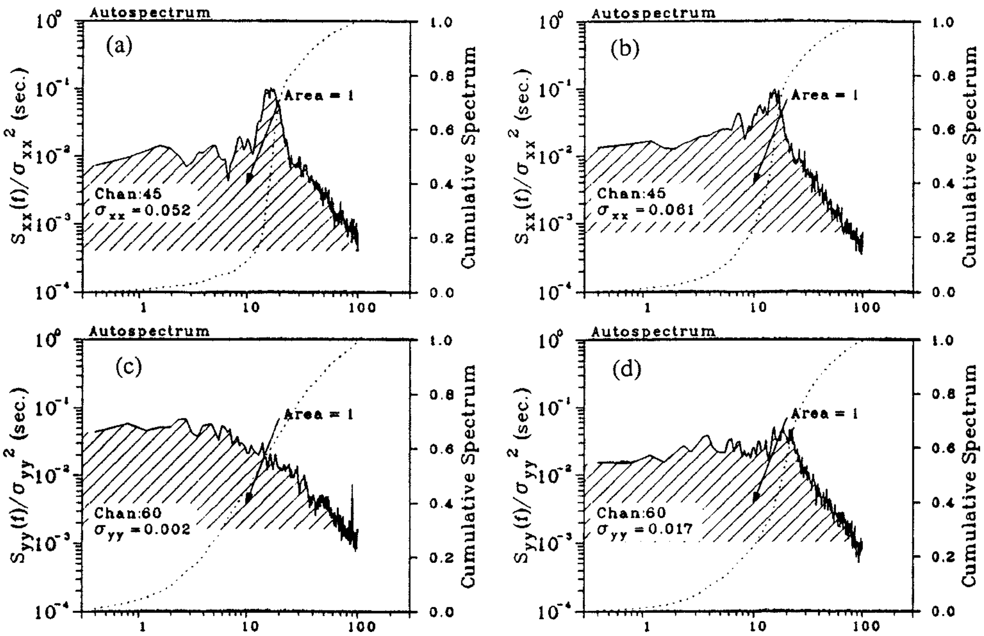

Fig. 8 Auto-spectra at a wind angle of 270° for (a) ring 1C in smooth flow (test B), (b) ring 1C in turbulent flow (test G), (c) ring 6A in smooth flow (test B) and (d) ring 6A in turbulent flow (test G)

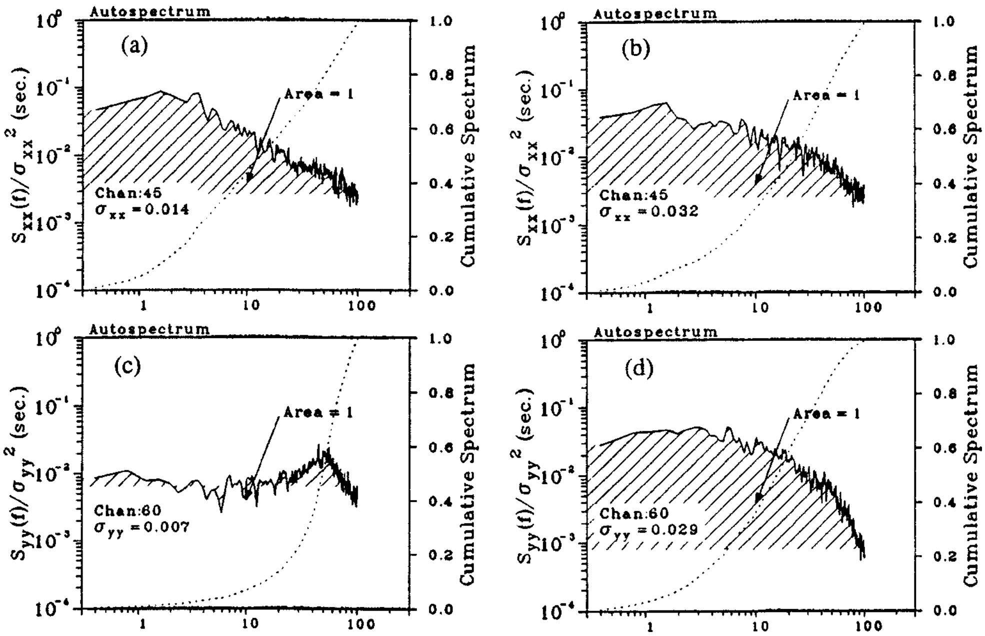

Fig. 9 Auto-spectra at a wind angle of 330° for (a) ring 1C in smooth flow (test B), (b) ring 1C in turbulent flow (test G), (c) ring 6A in smooth flow (test B) and (d) ring 6A in turbulent flow (test G)

implies a Strouhal number (fD/U) of 0.25. This rather high Strouhal number may be due to the local speed up of the wind through the array, which is not accounted for when the approach (i.e., tunnel) speed is used. In smooth flow, all six modules in the panel show the same spectral peak. However, module 1, which at this wind angle is down wind of module 6, shows a narrower peak than module 6. There is also more energy in the fluctuations with ring 1C having a rms. value of 0.030 while 6A has 0.004. Thus, the lock-in leads to more energetic fluctuations as the wind passes over the panel. This also occurs in turbulent flow, although more of the fluctuation energy results from turbulence, completely burying evidence of vortex shedding on the upwind module. This is consistent with the results obtained by Vickery (1981), who studied buffeting in a group of four in-line chimneys, and Hangan and Vickery (1999), who studied wake buffeting of two-dimensional sharp-edged cylinders. In fact, the centre-to-centre spacing of 2.25 D is close to the critical value of 2.5 found by Hangan and Vickery (1999), for two-dimensional bluff-bodies, and Havel *et al*. (2001), for three-dimensional surface mounted obstacles.

For a wind angle of 270°, shown in Fig. 8, the spectral peak due to vortex shedding is still evident, but is now observed at a frequency of about 15 Hz, so that the Strouhal number has changed to 0.075. This is likely due to change in the velocity normal to the modules because of the change in wind direction and/or change in the base pressure. Note also that the angle of attack is affected by a change in the wind direction. This was not investigated any further because the normalizing of C_T for module and declination angles was unsuccessful. (No attempt has been made to collapse the Strouhal number by taking into account the normal wind speed.) Other than the change in the Strouhal number, the results at 270° (Fig. 8) are similar to those at 225° (Fig. 7).

The spectra at 330°, shown in Fig. 9, are significantly different from those in the previous two figures. In this case the only evidence of vortex shedding is in the smooth flow case where modules 6−2 show vortex shedding (spectra for modules 5−2 are not shown). In the turbulent flow case, the turbulence energy swamps the vortex shedding fluctuations, so that no peaks due to vortex shedding are evident in any of the spectra.

Thus, recalling the mean and rms. torque coefficients in Fig. 6, wind from 270° and 330° both produce large loads, but through different mechanisms: for wind from 330°, through large mean torque and exposure to peak gusts; for wind from 270°, there is lower mean torque but each module has significant vortex shedding. Thus, in a final system evaluation, it is important to consider natural frequencies of the mechanical system to determine whether resonance (particularly with the vortex shedding) could enhance overall loading problems.

4.4. The effects of declination angle, module angle and wind angle

Figs. 10 and 11 summarize the absolute values of the peak torque coefficients, $|\hat{C}_{T,i}|$, for the seven tests where the subscript $i = 1$ to 6 correspond to the centreline rings of modules 1 to 6, the subscript "mod" means integration over the entire module (i.e., all five rings) and the subscript "array" means the simultaneous integration of the six midplane rings. Fig. 10 depicts the variation in the measured peak torque coefficients with γ, holding θ constant (for the worst case tested, $\theta = 75^{\circ}$). Fig. 11 depicts the variation in the measured peak torque coefficients with θ, holding γ constant (for the worst case tested, $\gamma = 45^{\circ}$). Examining Fig. 10, it is observed that the larger the declination angle, the larger the loads are. This makes sense physically because the larger the declination angle the more of the cross wind the individual modules "see" (except at wind angles near 90° and 270°). However, the dependence on declination angle is actually quite weak, especially comparing $\gamma = 30^{\circ}$ and 45°. An attempt to normalize the load coefficients with the velocity pressure normal to the modules had limited success and was not incorporated into the final simplified model of the results (discussed in (5)).

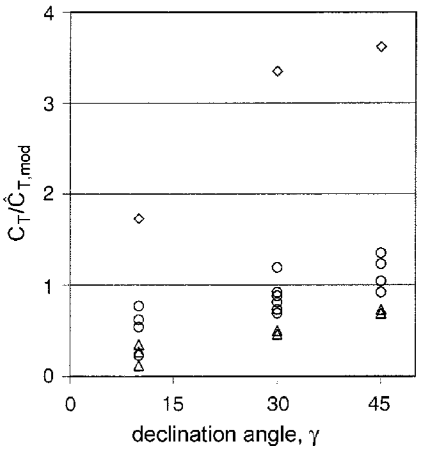

Fig. 10 Variation of peak torque coefficients with declination angle, γ : ○; $\hat{C}_{T,i}/\hat{C}_{T,\mathrm{mod}}$ for the six centreline rings, Δ ; $\hat{C}_{T,\mathrm{mod},i}/\hat{C}_{T,\mathrm{mod}}$ for the three modules with five rings (i.e., i = 1,2,4), ◇; $\hat{C}_{T,array}/\hat{C}_{T,\mathrm{mod}}$. The module angle, $\theta = 45^{\mathrm{o}}$

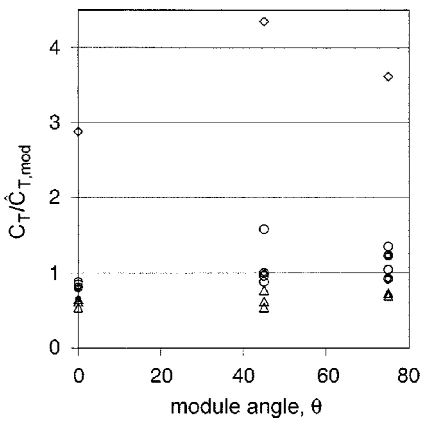

Fig. 11 Variation of peak torque coefficients with module angle, θ : ○; $\hat{C}_{T,i}/\hat{C}_{T,\mathrm{mod}}$ for the six centreline rings, Δ; $\hat{C}_{T,\mathrm{mod},i}/\hat{C}_{T,\mathrm{mod}}$ for the three modules with five rings (i.e., i = 1,2,4), ◇; $\hat{C}_{T,array}/\hat{C}_{T,\mathrm{mod}}$. The declination angle, $\gamma = 45^{\mathrm{o}}$

Observing Fig. 11, the effect of the module angle also appears to be small, at least when comparing differences between $\theta = 45^{\mathrm{o}}$ and 75^{o}. As with the declination angle, an attempt to normalize the load coefficients with the velocity pressure normal to the modules had limited success and was not incorporated into the final simplified model of the results. Clearly, the module angle of 0^{o} (at declinations used in North America) had the lowest loads, and it would be advisable in high winds to use this as the stopped configuration.

The results indicate a complex dependence on wind angle since a wide variety of wind angles are associated with the peak values. Table 2 summarizes the data in Figs. 10 and 11 with the other tests. Wind angles associated with the peak values are also given in the Table. Generally, the largest torque is observed for wind angles on or near the diagonals of the array, i.e., 45^{o}, 135^{o}, 225^{o}, and 315^{o}. However, the largest individual module torque is observed to occur at a wind angle of 270^{o} on module 4, which is in the centre of the panel. In this case, there is a lock-in of the vortex shedding which leads to the high loads as shown in Fig. 8. As to the effects of turbulence, it can be clearly observed in Figs. 10 and 11 that the turbulent flow case (test G) yields the largest peak torque coefficients, as expected.

Perhaps the most important data in Figs. 10 and 11 is that labeled $\hat{C}_{T,array}$. This data is summarized in Table 2 which also indicates the wind angles associated with the peak values. The array torque coefficient, $\hat{C}_{T,array}$, is the largest magnitude associated with the simultaneous integration of the six midplane rings (whose individual peak values are also listed in the table), i.e., 1C (module 1 - ring C), 2C, 3A, 4C, 5A and 6A. For example, consider test G. It is observed that the largest value of $\hat{C}_{T,array}$ occurs at a wind angle of 330^{o} while every other column indicates peak values at either 240^{o} or 270^{o}. Clearly, at 330^{o}, the loading from module to module must be more highly correlated than for wind angles near 240^{o}-270^{o}. It is also true that the peak values for individual rings at 330^{o} are also quite large, just not the largest observed.

Table 2 Absolute peak values of the torque coefficients, $\hat{C}_{T,i}$, for the midplane rings (1C, 2C, 3A, 4C, 5A, 6A), complete modules (1, 2, 4) and for the six midplane rings simultaneously. All coefficients are normalized by the largest module coefficient, $\hat{C}_{T,\mathrm{mod}} = 0.26$ (from module 4 in test G). The corresponding wind angles are shown in brackets

Test	γ	θ	$\hat{C}_{T,1}$	$\hat{C}_{T,2}$	$\hat{C}_{T,3}$	$\hat{C}_{T,4}$	$\hat{C}_{T,5}$	$\hat{C}_{T,6}$	$\hat{C}_{T,\mathrm{mod},1}$	$\hat{C}_{T,\mathrm{mod},2}$	$\hat{C}_{T,\mathrm{mod},4}$	$\hat{C}_{T,array}$
A	45°	0°	0.65 (90°)	0.81 (75°)	0.88 (135°)	0.81 (135°)	0.85 (75°)	0.88 (135°)	0.65 (90°)	0.54 (75°)	0.62 (30°)	2.88 (135°)
B	45°	75°	1.23 (240°)	1.35 (255°)	1.23 (240°)	0.92 (240°)	0.92 (180°)	1.04 (30°)	0.69 (240°)	0.73 (240°)	0.69 (180°)	3.62 (180° & 240°)
C	45°	45°	1.00 (180°)	0.96 (180°)	1.00 (67.5°)	1.00 (67.5°)	0.88 (180°)	1.58 (45°)	0.62 (180°)	0.54 (180° & 45°)	0.77 (45°)	4.35 (45°)
D	30°	45°	0.62 (67.5°)	0.77 (45°)	0.85 (45°)	0.88 (45°)	0.77 (67.5°)	0.77 (180°)	0.42 (67.5°)	0.50 (45°)	0.65 (45°)	3.65 (45°)
E	30°	75°	0.69 (158°)	0.88 (57.5°)	0.92 (45°)	0.73 (45°)	0.81 (158°)	1.19 (45°)	0.46 (158°)	0.46 (45° & 158°)	0.50 (180° & 22.5°)	3.35 (45°)
F	10°	75°	0.23 (0°)	0.62 (135°)	0.54 (113°)	0.54 (67.5°)	0.54 (67.5°)	0.77 (113°)	0.12 (22.5°)	0.35 (90°)	0.27 (67.5°)	1.73 (135°)
G	45°	75°	1.35 (270°)	1.88 (270°)	1.62 (240°)	1.23 (240°)	1.27 (240°)	1.35 (240°)	0.88 (240°)	0.96 (270°)	1.00 (270°)	5.23 (330°)

4.5. Peak correlation factors on individual modules

The fifteen largest values in the module torque coefficient time series, $C_{T,\mathrm{mod}}$, for each of the three modules with five rings (i.e., modules 1, 2 & 4) were evaluated in order to get a sense of how correlated these extreme events are along the span of the modules. The ratios of the peak module coefficients to the peak midplane coefficient were obtained, i.e.,

$$R_{T,\mathrm{mod}} = \frac{\hat{C}_{T,\mathrm{mod}}}{\hat{C}_{T,i}} \tag{4}$$

where the subscript "mod" is used for coefficients obtained over the entire module, i.e., all five rings, and the subscript "i" is used for coefficients obtained over only the midplane ring for the particular module in question. Thus, $\hat{C}_{T,i}$ is analogous to integration over the module with a single ring of taps with the implicit assumption of perfect correlation of pressure fluctuations along the length of the module. $R_{T,\mathrm{mod}}$ is an average of the fifteen largest peaks for the module in question.

Table 3 shows values of $R_{T,\mathrm{mod}}$ for wind angles 225°, 270° and 330° for the three fully instrumented modules. These values are remarkably high indicating that peak events tend to occur simultaneously across the span. This makes sense for the diagonal wind angles (225° and 330°) where there is, at best, a weak lock-in of the vortex shedding and it may be expected that a relatively large scale freestream fluctuation is the source of the peak loads. However, this is less important where vortex shedding is the primary mechanism (270°). Normally, for isolated cylinders, the vortex shedding process is correlated over only a very short span so that the correlation drops quickly to zero. Here, the correlation drops more rapidly for $\beta = 270°$ than for 330°, but is nevertheless still remarkably high.

Table 3 Estimates of correlation factors along a module during the peak events

Wind Angle / Flow Type	$R_{T,\,\mathrm{mod}}$ module 1	$R_{T,\,\mathrm{mod}}$ module 2	$R_{T,\,\mathrm{mod}}$ module 4
225°/smooth	0.75	0.76	0.64
225°/turbulent	0.72	0.55	0.57
270°/smooth	0.57	0.59	0.54
270°/turbulent	0.58	0.57	0.77
330°/smooth	0.89	0.90	0.85
330°/turbulent	0.79	0.75	0.76

Table 4 Estimates of the correlation factors between modules across the entire panel during the peak events

Wind Angle / Flow Type	$R_{T,\,array}$
225°/smooth	0.66
225°/turbulent	0.55
270°/smooth	0.50
270°/turbulent	0.43
330°/smooth	0.79
330°/turbulent	0.73

4.6. Peak correlation factors between modules

The fifteen largest peaks from the time series of the torque coefficient for the six midplane rings, $\hat{C}_{T,\,i}$, were evaluated along with those for the simultaneous integration of all six midplane rings (i.e., the “array” subscripts in Table 2) in order to get a sense of how correlated the peak events are between the modules. Ratios of the peak array coefficient to the sum of the six peak midplane coefficients were obtained, i.e.,

$$R_{T,\,array} = \frac{\hat{C}_{T,\,array}}{\sum_{i=1}^{N} \hat{C}_{T,\,i}} \tag{5}$$

where $N = 1$–6 and the peak coefficients are an average over the fifteen largest peaks. Table 4 shows values of $R_{T,\,array}$ for wind angles 225°, 270° and 330°. These values are reasonably high indicating that large events tend to occur simultaneously on each module of the array. The largest values are found for 330° indicating why this wind direction leads to the highest system torque. This likely occurs because the peak turbulent fluctuations in the oncoming flow are of large scale, in combination with high mean torques.

5. A simplified model of C_T

The results shown thus far have a relatively strong dependence on wind angle, as the spectra and peak torque coefficients clearly indicate. On the one hand, the largest system torque occurs at a wind angle of 330°. At this wind angle the modules exhibit little evidence of vortex shedding. The peak events exhibit a significant correlation over the panel so that $\hat{C}_{T,array}$ is large. On the other hand, there is a large system torque at a wind angle of 270° where there is significant locked-in vortex shedding. Interestingly, the overall torque, indicated by $\hat{C}_{T, array}$ is less than that for 330° although the individual modules all have higher peak values and the vortex shedding is well correlated.

In order to make the most use of the results for design, a simplified model is investigated, based on the following hypotheses: (i) The mean loading is not very sensitive to turbulence level. (ii) The effect of the turbulence is effectively quasi-steady (i.e., aside from the vortex shedding, the peak unsteady load is proportional to a suitably chosen peak wind dynamic pressure). (iii) The effect of vortex shedding is not dramatically altered by the presence of turbulence and is essentially dependent on the large-scale quasi-steady wind speed. Hence, these effects can be added together. Note that the full scale vortex shedding would be expected to occur at a frequency of about 5 Hz, assuming a Strouhal number of 0.075 and a wind speed of about 30 m/s. Thus, many cycles occur within a representative 3-second wind gust.

It should also be recalled, as discussed in the introduction, that although solar arrays are placed in a wide variety of locations, each with a different orientation and surrounding environment, this effect on the load is neglected. However, the appropriately chosen wind speed should consider any possible speed-up which may occur when the array is placed near the edge of a roof. Rather than investigate the overall effect of wind angle on the aerodynamic torque coefficient, we will examine only the three wind angles discussed thus far with the intention of estimating only the peak torque coefficient, $\hat{C}_T$.

Starting with Eq. (2), we note that the peak torque for a single ring of taps on a module is

$$\hat{T} = \hat{C}_T \hat{q} L D^2 \tag{6}$$

since $\hat{T}$ can legitimately occur due to vortex shedding induced fluctuations and also due to turbulent fluctuations in q. Assuming the peak turbulent fluctuation of velocity and a vortex shedding peak value occur simultaneously to create the worst case, we can write

$$\hat{T} = (\hat{C}_{T,i} + g_1 C'_{T,VS})\left[\frac{1}{2}\rho(U + g_2 u')^2\right] L D^2 \tag{7}$$

where u' is the streamwise rms. velocity, $\hat{C}'_{T,VS}$ is the rms. torque due to vortex shedding (which is obtained from smooth flow data, a typical value for strong shedding being 0.035, cf. Fig. 6), g_1 and g_2 are peak factors for vortex shedding and turbulence in the approach flow; $g_1 \sim \sqrt{2}$ and $g_2 \sim 3{-}4$. Here, $\hat{C}_{T,i}$ is the peak torque coefficient from a single ring with the vortex shedding effects removed. Re-arranging and neglecting the second order fluctuating terms, we obtain

$$\hat{T} = \hat{C}_{T,i} \bar{q} L D^2 \left[1 + g_1 \frac{C'_{T,VS}}{\hat{C}_{T,i}} + 2 g_2 I\right] = \hat{C}_T \bar{q} L D^2 \tag{8}$$

where

$$\hat{C}_T = \hat{C}_{T,i}\left[1 + g_1 \frac{C'_{T,vs}}{\hat{C}_{T,i}} + 2 g_2 I\right] \tag{9}$$

For an array with N modules (i.e., $N = 6$ in the present configuration), we add the module and array correlation factors such that

$$\hat{C}_T = N\hat{C}_{T,i}\left[1 + g_1 \frac{C'_{T,vs}}{\hat{C}_{T,i}} + 2 g_2 I\right] R_{T,array} R_{T,\mathrm{mod}} \tag{10}$$

where N is the number of modules, $R_{T,array}$ is a correlation factor for the peak loads across the panel, and $R_{T,\,\mathrm{mod}}$ is a correlation factor along a module. With estimates obtained for $\hat{C}_{T,\,i}$ (cf. Table 2), $C'_{T,\,vs} \approx C'_{T,\,i}$ (cf. Fig. 6; smooth flow), $R_{T,\,array}$ (cf. Table 4) and $R_{T,\,\mathrm{mod}}$ (cf. Table 3), estimates of the peak factors can be obtained with the peak factor for vortex shedding, g_1, obtained from the smooth flow conditions. Following this, the peak factor for the turbulence level, g_2, can be obtained. By applying Eqs. (2) and (10) to the data, we found that $g_1 \sim 1.5$ and $g_2 \sim 3$, as expected, provide a good fit for the data (Kopp and Surry 1998). For design, it is recommended that the largest magnitudes of $\hat{C}_{T,\,i}$, $R_{T,\,array}$, and $R_{T,\,\mathrm{mod}}$ be used.

6. Conclusions

The aerodynamically-induced torque on a solar panel containing six slender, parallel modules was investigated. It was found that the peak torque was largest at two particular wind angles that exhibited drastically different phenomena. At a wind angle of 270^o, there was a strong lock-in of the vortex shedding which allowed a high correlation of the fluctuating torque coefficient even though the mean coefficients were relatively small. Spacing between modules was observed to be at approximately the critical value for wake buffeting, which accounts for the observed lock-in of the vortex shedding. In contrast, at a wind angle of 330^o, there was no evidence of vortex shedding and the peak loads were due primarily to large scale turbulence in the oncoming flow.

A simplified, linearized model was developed to predict the peak system torque. This model takes into account the effects of vortex shedding and freestream turbulence intensity. Additional factors include the correlation of extreme events along the modules and across the panel between modules. The model assumes the worst wind angle rather than taking into account the variation of the mean torque coefficient with wind angle, declination angle and module angle. This allows a designer to estimate the worst case system torque in conjunction with an appropriately chosen oncoming mean velocity and turbulence intensity.

The simplified model can also be used as a guide to reduce the wind-induced torque. For example, at a wind angle of 330^o, the peak torque is due primarily to the mean coefficient, $\bar{C}_T$, and the freestream turbulence intensity. In this case, savings could come from optimizing the location of the centre of rotation. On the other hand, for a wind angle of 270^o, the torque is induced primarily by vortex shedding. This could be substantially reduced by utilizing splitter plates, or some other aerodynamic technique, to hinder the vortex shedding process (at the cost of possibly higher frame loads).

References

Cochran L. (1986), "Influence of porosity on the mean and peak wind loads for three concentrator photovoltaic arrays", MESc Thesis, Colorado State University.

Hangan, H. and Vickery, B.J. (1999), "Buffeting of two-dimensional bluff bodies", *J. Wind Eng. Ind. Aerod.*, **22**, 173-187.

Havel, B., Hangan, H. and Martinuzzi, R.J. (2001), "Buffeting for 2D and 3D sharp-edged bluff bodies", *J. Wind Eng. Ind. Aerod.*, **89**, 1369-1381.

Kopp, G.A. and Surry, D. (1998), "Measurements of aerodynamic loads on a linear concentrator photovoltaic array", *Boundary Layer Wind Tunnel Laboratory Report BLWT-SS37-1998*.

Peterka, J.A. and Derickson, R.G. (1992), "Wind load design methods for ground based heliostats and parabolic dish collectors," *Sandia National Laboratories Report SAND92-7009*.

Vickery, B.J. (1981), "Across-wind buffeting in a group of four in-line model chimneys", *J. Wind Eng. Ind. Aerod.*, **8**, 177-193.

AK